ZIBELINE INTERNATIONAL™ PUBLISHING

Pakistan Journal of Geology (PJG)

DOI: http://doi.org/10.26480/pjg.01.2023.11.20

ISSN: 2521-2915 (Print)
ISSN: 2521-2923 (Online)
CODEN: PJGABN

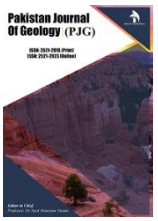

RESEARCH ARTICLE

REGRESSION MODELLING OF THE ACCURACY OF GNSS REAL TIME KINEMATIC OBSERVATIONS REFERENCED TO SACREDION TERSUS GEOBEE30 CORS

Chika Vincent Okorocha[a], Stephen Olushola Oladosu[b], Raphael Ehigiator-Irughe[b]

[a]Department of Civil Engineering, Faculty of Engineering, University of Benin, P.M.B. 1154, Edo State.
[b]Department of Geomatics, Faculty of Environmental Sciences, University of Benin, P.M.B. 1154, Edo State.
[*]Corresponding Author Email: olushola.oladosu@uniben.edu

ARTICLE DETAILS

Article History:

Received 25 June 2023
Revised 28 July 2023
Accepted 01 September 2023
Available online 09 September 2023

ABSTRACT

This research employs a regression model to verify the accuracy of the Sacredion Tersus GeoBee30 CORS in real-time kinematic mode. This verification process entails utilizing differential correction broadcasted through the internet protocol (NTRIP) to the GNSS rover. Given Nigeria's current demand for additional CORS to enhance geospatial services, the primary objective of this study is to determine the strength of signal coverage, which is crucial for strategically locating appropriate or estimated location for the installation of new CORS. The methodology involves conducting an independent observation session at 5 minutes on 14 temporary points, away from the CORS base. The analysis, carried out using one-way ANOVA, establishes the fact that the RTK observations referenced to the CORS exhibit high precision. Furthermore, the development of a linear regression model yields a robust positive correlation, underscoring the dependable link between the investigated RMS error and the observed distances (RMSE = 0.988; R-square = 0.977; adjusted R-square = 0.976) within the distance range of 75 km target, extended to 120 km by prediction. The rms values of 0.0093 m were discovered in both cases while testing the efficacy of the prediction model on two known ground controls within the study area. In conclusion, this study unequivocally confirms the accuracy of the CORS, thereby endorsing its suitability for tasks involving mapping and geomatics activities, not only within the verified 70-km range but also beyond it. There exist a linear relationship between the distance coverage and the RMS error in relative positioning to the CORS at 95% confidence interval (α = 0.05 significant value). However, we do not have enough evidence to reject the null hypothesis outrightly.

KEYWORDS

CORS, Distance, GNSS, NTRIP, Positioning, Regression

1. INTRODUCTION

Continuously observing reference stations can be improved through various methods. One approach is to employ a system that includes a reference station, a rover, and a base station (Wu et al., 2017). One such approach involves the integration of a comprehensive system consisting of a reference station, a rover, and a base station (Wu et al., 2017). The base station plays a crucial role by receiving vertical error data from the reference station and subsequently adjusting the GNSS antenna to minimize errors (Shuguang et al., 2017). Another effective method utilizes Principal Component Analysis (PCA) to mitigate common mode errors present in the coordinate time series of reference stations (Liu et al., 2015; Dai et al., 2014). Additionally, accounting for the influence of diverse surface mass loadings on station displacement contributes to addressing common mode errors (Hu et al., 2018; Lau and Kai-Wing, 2023). A CORS data broadcasting system can also be implemented to reduce distribution costs and improve the quality of CORS data (Kolopaking, 2018). Furthermore, a continuously operating reference station system can utilize a network device to transmit correction data to a client application subsystem, enabling the display of positioning results on terminal devices (Khai and Long, 2019).

CORS form a network of stations strategically positioned to supply data from global navigation satellite systems. This dataset includes meticulous measurements of carrier phase and code range, intended to support a range of applications including three-dimensional positioning, climate change, sea level rise, meteorology, space weather, and geophysics. The CORS network boasts a remarkable expanse, encompassing more than 2000 stations, each contribution hailing from distinct organizations. This collaborative initiative continues to drive the network's growth, perpetuating its widespread influence and utility (Botsyo et al., 2020, Hernández-Andrade et al., 2022).

The advent of the Global Navigation Satellite System (GNSS) has ushered in a paradigm shift in traditional methods of position determination and navigation techniques (Omogunloye et al., 2017: Jaskowski, 2022). In Real-Time Kinematic (RTK) mode, a GNSS rover obtains differential correction from a base station via radio, yet its accuracy is susceptible to several errors, including multipath effects, ionospheric and tropospheric errors, obstruction in radio communication between the base and rover during correction transmission, and various environmental influences and so on (National Geodetic Survey [NGS], 2021).

The concept of utilizing a single base-to-rover system in RTK mode has been firmly established for over two decades (Janssen and Haasdyk, 2011). For instance, Jaskowski et al. (2021) introduced a model that employed a mobile GNSS RTK rover to assess the lighting characteristics of street lights along a road section. They demonstrated that the post-measurement field analysis method offered a prompt and reliable means to replicate street light conditions. Nordin et al. (2021) performed GNSS RTK-based observations for varying time intervals, culminating in the noteworthy conclusion that the RTK-based approach attains precision

Quick Response Code	Access this article online	
	Website: www.pakjgeology.com	**DOI:** 10.26480/pjg.01.2023.11.20

Cite The Article: Chika Vincent Okorocha, Stephen Olushola Oladosu, Raphael Ehigiator-Irughe (2023). Regression Modelling of The Accuracy of Gnss Real Time Kinematic Observations Referenced to Sacredion Tersus Geobee30 Cors. *Pakistan Journal of Geology, 7(1): 11-20.*

levels up to an impressive 2 cm accuracy.

Additionally, Li et al. (2019) conducted an in-depth investigation of signal blockage in RTK carrier mode and revealed that signal interruptions lasting 10 to 15 seconds had a negligible impact on the centimeter-level accuracy of fixed positions, with more than 94% of carrier phase errors exhibiting minimal effects. To analyze four crucial environmental factors, Mendez-Astudillo et al. (2021) artfully employed an algorithmic approach, yielding an impressive accuracy of 1.71 °C at a 95% confidence level based on the validation results using archived data. On the other hand, Pirti and Hosbas (2019) diligently measured seventeen points distributed across obstructed and unobstructed locations to gauge the accuracy of the RTK mode. The findings accentuated discrepancies in centimeter-level accuracy between obstructed and unobstructed locations, a common occurrence in cases characterized by limited satellite availability.

It is widely acknowledged that the introduction of a single CORS will not only serve a comparable purpose to the traditional base-to-rover systems but also provide the added advantage of enabling simultaneous connections for multiple users (Oladosu et al., 2022). In both approaches, distance-dependent error corrections are seamlessly disseminated to the user(s) from either the base station or the single CORS. Nonetheless, a limitation of these techniques lies in their inability to provide extensive coverage beyond 20 km, as asserted by (Janssen and Haasdyk, 2011). However, Zhang et al. (2006) contended that under conditions of minimal ionospheric impact and meticulous error modeling, this range could potentially extend up to 50 km, signifying a substantial improvement.

As technological breakthroughs continue to shape the field, the network RTK (NRTK) approach has experienced remarkable progress, furnishing highly accurate position solutions across diverse applications on a global scale. The baseline established by the separation between the rover and the base station is a position vector with an origin at the base station or the single CORS (Oladosu et al., 2022). Thus, the position vector of the rover station defines the DGNSS baseline (range vector). The accuracy of the determined position in DGNSS positioning is impacted by the baseline length, and this accuracy depends on the satellite geometry (Omogunloye et al., 2017). It is also worthwhile to note that satellite geometry has an amplifying effect on other GNSS sources of error (Lonchay, 2009).

Recent literature on research relying on CORS applications includes a study by Agca and Daloglu (2023), who evaluated the accuracy of geoid height points using various data sources, especially from GNSS/CORS, verified by three different methods. The results showed that the height relationship between Lidar ICESat-2/ATLAS is better than the height relationship obtained between GNSS/CORS-ICESat-2/ATLAS in Turkey. Erekosima and Onoriode (2018) presented a paper at the FIG congress in Istanbul, Turkey, which took place between May 6 and May 11, discussing the use of GNSS/CORS technology in Nigeria's oil and gas industry and how the innovation has changed the mapping system and improved health, safety, security, and the environment through fast, accurate, and timely service delivery. Omogunloye et al. (2017) determined the difference between the level of standard error obtained in short (1.5 km), medium (12 km), and long (107 km) baseline processing involving the CORS technology. The findings revealed that, while the short and medium baselines processing did not differ significantly, the long baselines processing showed significant difference.

The majority of previous studies investigated (Janssen and Haasdyk, 2011; Hamish, 2004; Fotiou et al., 2006; Omogunloye et al., 2017) have demonstrated the presence of error sources affecting GNSS/CORS positioning with particular focus on the orbital errors and atmospheric errors (i.e., the combined ionospheric and tropospheric errors). However, investigating the RTK accuracy with regression modeling of segmented distances from a single CORS is still vague. As a result, this study focuses on the effect of distances on the accuracy of the RTK mode data acquisition system extended over long coverage distance. The root mean square (RMSE) of CORS observations is affected by the distance from a continuously operating reference station CORS. The error propagation approach was used to estimate the RMSE of alternative data for calculating reference evapotranspiration (ET0). The results showed that the RMSE is proportional to the value produced by the error propagation approach (ΔET0) (Ferreira et al., 2021). The invention of a CORS data coding and transmitting method using Beidou CORS vehicles and high-power ultra-short-wave radio sets allows for reliable transmission of CORS data over long distances, reducing the bit error rate and improving communication quality (Paquet, 1980: Jing-Xiang and Hong, 2009).

The root mean square (RMS) of CORS observations is affected by the distance from a continuously operating reference station (CORS). The variations in station coordinates deduced from Doppler observations using a single point positioning method show a coherence generally better than 1 m, but occasionally differences of 1.5 or 3 m can be detected (Paquet, 1980). The study of filtering problems for Markov jump linear systems (MJLSs) suggests that an optimal linear filter for the mode operation could be more favorable in the solution of the control problem with partial observations (Fortia and Marcelo, 2019). Data assimilation plays a crucial role in estimating observation error covariance matrices, which are important for the quality of the analysis (Homayoon and Takamitsu, 2019). Formulas have been derived to calculate the RMS displacement, slope, and curvature errors in an azimuth-elevation image trace of an elongated object in space, providing useful measures for determining the relative merits of different triangulation procedures (Long, 1974). The estimation of reference evapotranspiration (ET0) using alternative data can be validated by calculating the root mean square error (RMSE), which is proportional to the value produced by the error propagation approach (Homayoon and Takamitsu, 2019).

This research aims to assess the precision and accuracy of GNSS differential corrections from CORS over long-range distances in RTK mode. To achieve this, a regression modeling approach was applied to the observed data, and the relative positioning accuracy of the rover receiver at various distances was determined in an interval of 5 km each from the Sacredion Tersus GeoBee30 CORS, hereafter abbreviated as (STGBC). Predictions of higher distances up to 120 km was also achieved.

2. Materials and Methods

2.1 Study Area

This research was carried out in Lagos State, Nigeria. The STGBC antenna is located in number 50 Toyin Street in Ikeja. Figure 1 shows the study area and the preliminary buffer spread from the CORS reference station to the final destination in Google Earth Pro Landsat image. The boundary coordinates are: (3°59'3.70"E, 6°34'48.70"N; 3°20'41.70"E, 6°35'55.65"N).

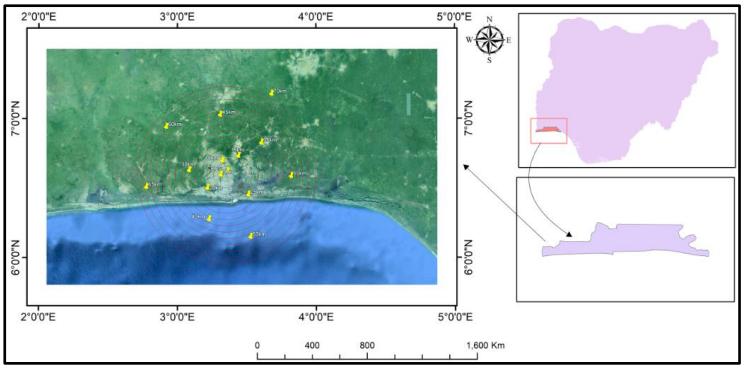

Figure 1: Study area map

2.2 STGBC Peculiarity

The Reference station adopted for this research work is the STGBC is a smart CORS with the coordinates of its location specified as: (539063.9258 mE; 728901.7681 mN) and has its orthometric height as 45.22 m above mean sea level. The STGBC is a dedicated and cost-effective solution for transmitting and receiving correction from Networked Transport of Radio Technical Commission for Maritime Services Internet Protocol (NTRIP) data transmission. With Tersus NTRIP Caster Service, NTRIP Modem and David30 GNSS Receiver, the STGBC opens the possibility for users to transmit (RTK) corrections via Internet (Ethernet or 2G/3G/4G) in a simple, user friendly, by simply inserting a SIM card or by using Ethernet

cable without the need for a static IP (https://www.tersus-gnss.com/product/geobee30). The Tersus Oscar Basic GNSS rover system is a multi-constellation multi-frequency (MCMF) satellite positioning system with over 500 satellite channels receiving satellite positioning information from GPS, GLONASS, GALILEO and BEIDUO simultaneously. All GNSS rovers from different manufacturers that receive NTRIP corrections can easily connect to the network for various surveying applications. Plate 1 shows the picture of the roof-top-mounted STGBC antenna location. More information can be found at (https://www.tersus-gnss.com/product/geobee30).

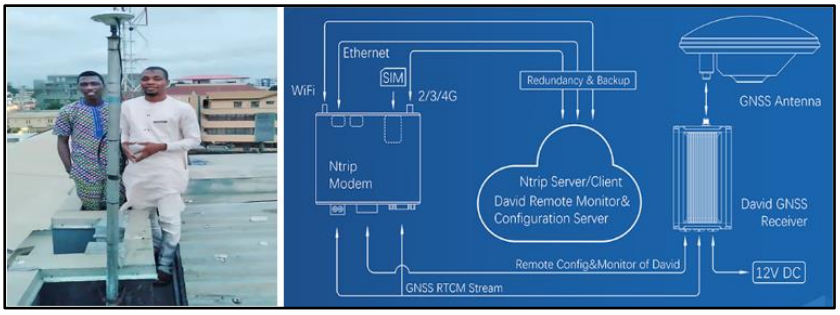

Plate 1: STGBC location and NTRIP server

2.3 Pseudo-Range Measurement

The principle of measurement between a CORS and a rover system rely on the popular pseudo-range measurement equations. The limitation of using base-rover system is the inability to cover more than 10 km without the introduction of distance-dependent biases (errors) like the combine atmospheric error (i.e. ionospheric, tropospheric), orbital error etc. The invention of CORS technology mitigate this limitation by modelling the error from the measurement obtained by the rovers to cover as much as 70 km as we have in this research. Figure 2 is an example of pseudo range measurement style between the satellite in space and an observer with rover receiver on Earth's surface. With a minimum of four (4) satellites position can be fixed but ideally the more the number of satellites tracked the better the positioning accuracy.

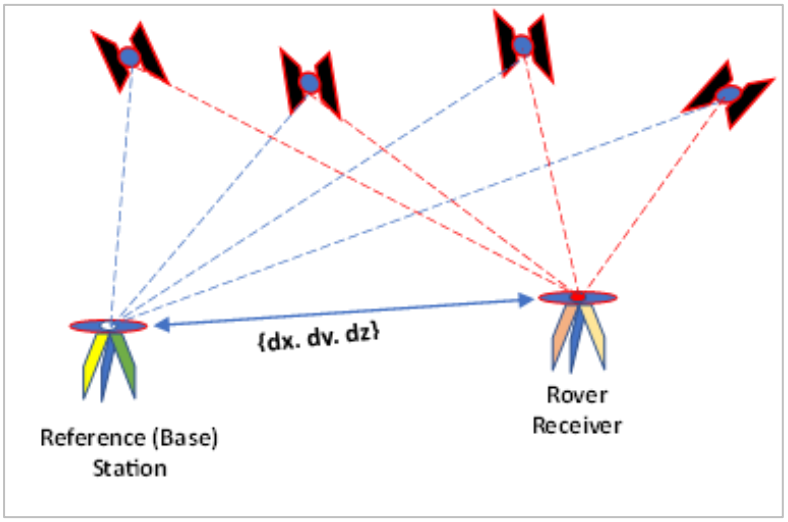

Figure 2: Working principle of the RTK virtual positioning technique

The pseudo-range equation for this scenario can be formulated between the satellite and the observer at a given epoch in carrier phase measurement while the rover is receiving corrections from the CORS as shown in Equation 1 (European Space Agency, {ESA, 2018}).

$$\phi = \rho - I + Tr + C(b_{Rx} - b_{Sat}) + N\lambda + \varepsilon_{\phi} \quad (1)$$

Where: I, is the signal path delay due to the ionosphere; Tr, is the signal path delay due to the troposphere; b_{Rx}, is the receiver clock offset from the reference (GNSS) time; b_{Sat}, is the satellite clock offset from the reference (GNSS) time; C, is the speed of light in air; λ, is the carrier nominal wavelength; N, is the ambiguity or integer number in the carrier-phase; ε_{ϕ}, are the measurement noise components; ρ, is the geometrical range between the satellite and the rover receiver. The position solution is a function of the satellite $(x_{Sat}, y_{Sat}, z_{Sat})$ and the receiver (x_{Rx}, y_{Rx}, z_{Rx}) as presented in Equation 2 (ESA, 2018).

$$\rho = \sqrt{(x_{Sat} - x_{Rx})^2 + (y_{Sat} - y_{Rx})^2 + (z_{Sat} - z_{Rx})^2} \quad (2)$$

For multiple distances with rover receiver taking observation on temporary stations, equation 2 can be re-projected as shown in Equation 3.

$$\rho_1 = \sqrt{(x_{Sat} - x_{R1})^2 + (y_{Sat} - y_{R1})^2 + (z_{Sat} - z_{R1})^2}$$
$$\rho_2 = \sqrt{(x_{Sat} - x_{R2})^2 + (y_{Sat} - y_{R2})^2 + (z_{Sat} - z_{R2})^2}$$
$$\rho_3 = \sqrt{(x_{Sat} - x_{R3})^2 + (y_{Sat} - y_{R3})^2 + (z_{Sat} - z_{R3})^2}$$
$$\rho_{70} = \sqrt{(x_{Sat} - x_{R70})^2 + (y_{Sat} - y_{R70})^2 + (z_{Sat} - z_{R70})^2} \quad (3)$$

2.4 Project Design and Data Acquisition

The project was designed such that observations were taken in successions. First, the distances for the rover to acquire data relative to the STGBC was set at the controller interface and a survey grade Toyota highlander jeep was drove along an existing route to the successive temporary stations. The STGBC being the origin (zero), data taken commences at distances 5 km, 10 km, 15 km, and so on to the last point 70 km away from the STGBC. The interval of 5 km signifies a total of fourteen (14) temporary stations were marked with red paint along the route for easy identification. Three set of observation sessions were performed using the NTRIP RTK technique while placing the rover on the temporary marked stations with occupation time (duration) of 5 minutes on each station. In this manner, necessary data were acquired for subsequent use in analysis. Figure 3 is a conceptual design of the data acquisition approach.

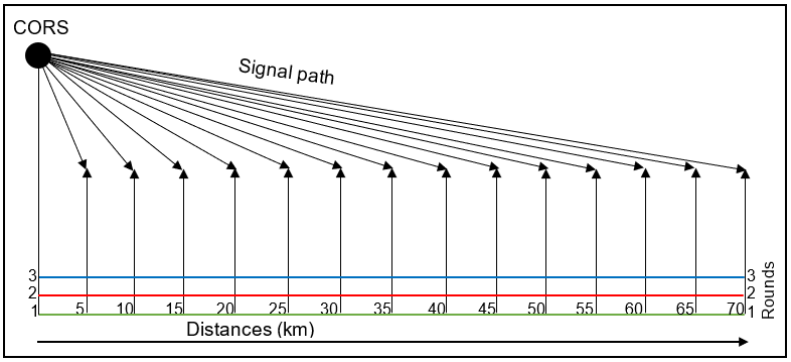

Figure 3: Conceptual design for data acquisition

2.5 Linear Regression Model

Linear regression creates a mathematical linear model for determining the relationship between two sets of observations or quantities for the purpose of effectively predicting the result of an observation from the independent variables. In this case the determinant quantity is the coverage distance while the positioning error is the quantity to be predicted. The linear regression was conducted at 95% confidence interval. Since there is precision in the positioning error to the STGBC, the average of the three rounds of errors was used in developing the linear regression model. Consider a regression model given in equation 4.

$$Y = aX + b \quad (4)$$

Where Y = predicted variable (dependent variable)

X = coverage distance (independent variable)

a = the slope of the line of best fit

b = the intercept of the regression line

2.6 Hypothesis Testing

The null and alternative hypothesis were set and tested as follows.

2.6.1 Null Hypothesis Ho

There is no linear relationship between the distance coverage and the RMS error in relative positioning to the STGBC at 95% confidence interval (α = 0.05 significant value). This hypothesis is accepted if P Value ≥ α otherwise reject.

2.6.2 Alternative hypothesis H_A

There is a linear relationship between the distance coverage and the RMS error in relative positioning to the STGBC at 95% confidence interval (α = 0.05 significant value). This hypothesis is accepted if P Value ≤ α otherwise reject.

3. Results and Discussions

The results obtained are presented using various tables and charts. Tables 1 to 3 represent the beginning point of observation to the end point (i.e. end-to-end) for the three set of observation sessions. In the Tables, the coverage distance, the 2D coordinates, the orthometric, and ellipsoidal heights have slight differences after the decimal separations. However, the hrms, vrms, and the rms errors are different in each cases. Station 1 having 5 km buffer from the STGBC has the least hrms, vrms, and rms respectively. The station 14 having 70 km buffer from the STGBC has the highest hrms, vrms, and rms. A critical study of the three Tables also reveals that the error rate increases steadily with coverage distances. This confirm a form of linear and progressive error propagation with distances. The end-to-end positional accuracy was further averaged and the result presented in Table 4.

Table 1: End-To-End First Round of Observations

Station	Coverage (km)	Northings (m)	Eastings (m)	Orthometric Height (m)	Ellipsoidal Height (m)	hrms (m)	vrms (m)	rms (m)
1	5	730331.1847	543855.2916	13.5585	36.7033	0.0061	0.0084	0.0104
2	10	730744.1936	548889.3428	2.7387	25.8859	0.0076	0.0093	0.0120
3	15	732254.6004	553678.0069	5.0643	28.2727	0.0107	0.0162	0.0194
4	20	732928.6209	558649.4398	35.2908	58.5295	0.0111	0.0133	0.0173
5	25	734785.9229	563351.9143	13.9954	37.3287	0.0129	0.0210	0.0246
6	30	736509.0812	568071.5958	29.7169	53.1399	0.0175	0.0327	0.0371
7	35	737594.3393	572952.9926	31.2250	54.6961	0.0166	0.0285	0.0330
8	40	734964.7369	578585.4547	33.5988	56.9572	0.0261	0.0377	0.0459
9	45	734658.9559	583676.9068	13.3617	36.7089	0.0253	0.0317	0.0406
10	50	760834.6815	577515.2933	63.6288	87.8744	0.0300	0.0377	0.0482
11	55	734473.7839	593761.102	7.3387	30.6814	0.0266	0.0410	0.0489
12	60	753281.1416	593864.4488	42.5225	66.4395	0.0290	0.0362	0.0464
13	65	751223.3529	600086.6616	25.1397	48.9543	0.0315	0.0415	0.0521
14	70	728757.758	609038.5472	25.7814	48.8746	0.0321	0.0494	0.0589

Table 2: End-To-End Second Round of Observations

Station	Coverage (km)	Northings (m)	Eastings (m)	Orthometric Height (m)	Ellipsoidal Height (m)	hrms (m)	vrms (m)	rms (m)
1	5	730331.1859	543855.2936	13.5681	36.7129	0.0058	0.0078	0.0097
2	10	730744.1976	548889.3486	2.7329	25.8801	0.0075	0.0091	0.0118
3	15	732254.5825	553678.0083	5.0248	28.2332	0.0109	0.0176	0.0207
4	20	732928.6308	558649.4369	35.297	58.5357	0.0112	0.0132	0.0173
5	25	734785.9099	563351.9179	14.0209	37.3542	0.0128	0.0209	0.0245
6	30	736509.0893	568071.5895	29.7558	53.1788	0.0156	0.0260	0.0303
7	35	737594.3447	572952.9877	31.2476	54.7187	0.0163	0.0275	0.0320
8	40	734964.7317	578585.4524	33.6135	56.9719	0.0216	0.0260	0.0338
9	45	734658.9581	583676.9256	13.3365	36.6837	0.0248	0.0324	0.0408
10	50	760834.6712	577515.3301	63.5903	87.8359	0.0277	0.0316	0.0420
11	55	734473.7749	593761.1061	7.3877	30.7304	0.0268	0.0386	0.0470
12	60	753281.2784	593864.3094	42.0868	66.0038	0.0290	0.0366	0.0467
13	65	751223.3684	600086.6886	25.1432	48.9578	0.0319	0.0422	0.0529
14	70	728757.7788	609038.5233	25.8002	48.8934	0.0321	0.0514	0.0606

Table 3: End-To-End Third Round of Observations

Station	Coverage (km)	Northings (m)	Eastings (m)	Orthometric Height (m)	Ellipsoidal Height (m)	hrms (m)	vrms (m)	rms (m)
1	5	730331.188	543855.294	13.5	36.7	0.0055	0.0073	0.0091
2	10	730744.194	548889.358	2.8	25.9	0.0075	0.0095	0.0121
3	15	732254.551	553678.005	5.1	28.3	0.009	0.0158	0.0182
4	20	732928.629	558649.448	35.3	58.5	0.0111	0.0131	0.0172
5	25	734785.900	563351.928	13.9	37.3	0.0126	0.0210	0.0245
6	30	736509.087	568071.585	29.8	53.2	0.0158	0.0261	0.0305
7	35	737594.352	572952.990	31.3	54.7	0.0164	0.0263	0.0310
8	40	734964.745	578585.464	33.6	56.9	0.0225	0.0260	0.0344
9	45	734658.953	583676.967	13.3	36.7	0.0250	0.0325	0.0410
10	50	760834.676	577515.339	63.6	87.8	0.0273	0.0317	0.0418
11	55	734473.758	593761.110	7.4	30.8	0.0270	0.0366	0.0455
12	60	753281.373	593864.253	41.8	65.7	0.0291	0.0377	0.0476
13	65	751223.367	600086.692	25.1	48.9	0.0306	0.0402	0.0505
14	70	728757.793	609038.504	25.8	48.8	0.0328	0.0503	0.0600

Table 4: End-To-End Averaged Positioning Accuracy Information

Station	Coverage (Km)	Northings (m)	Eastings (m)	Orthometric Height (m)	Ellipsoidal height (m)	Average hrms (m)	Average vrms (m)	Average rms (m)
1	5	730331.188	543855.294	13.5	36.7	0.00580	0.00783	0.00973
2	10	730744.194	548889.358	2.8	25.9	0.00753	0.00930	0.01196
3	15	732254.551	553678.005	5.1	28.3	0.01020	0.01653	0.01943
4	20	732928.629	558649.448	35.3	58.5	0.01113	0.01320	0.01726
5	25	734785.900	563351.928	13.9	37.3	0.01276	0.02096	0.02453
6	30	736509.087	568071.585	29.8	53.2	0.01630	0.02826	0.03263
7	35	737594.352	572952.990	31.3	54.7	0.01643	0.02743	0.03200
8	40	734964.745	578585.464	33.6	56.9	0.02340	0.02990	0.03803
9	45	734658.953	583676.967	13.3	36.7	0.02503	0.03220	0.04080
10	50	760834.676	577515.339	63.6	87.8	0.02833	0.03366	0.04400
11	55	734473.758	593761.110	7.4	30.8	0.02680	0.03873	0.04713
12	60	753281.373	593864.253	41.8	65.7	0.02903	0.03683	0.04690
13	65	751223.367	600086.692	25.1	48.9	0.03133	0.04130	0.05183
14	70	728757.793	609038.504	25.8	48.8	0.03233	0.05036	0.05983

3.1 Comparative Analysis of the Horizontal, Vertical and Rms Errors

The accuracy obtained for the three sessions were compared in terms of their hrms, vrms, and rms. The results are shown in Figures 4 to 6.

Figure 4 shows the hrms accuracies of the three observation sessions. At station 3 (15 km), first and second round of observation are very close but the third observation deviate with value less than 0.01 m. At station 6 (30 km) second and third round of observations were very close, but the first observation deviate with higher value. At station 8 and 10 (40 km and 50 km) while the second and the third round of observations were close, the first observation deviated somewhat higher. The linear graphical illustrations at a glance show a continuous increase in the positioning accuracy from 5 km to 75 km. The horizontal accuracy ranges from 0.005 m to 0.03 m.

Figure 5 shows the vrms accuracies of the three observation sessions. At station 3 (15 km), little deviation exists among the three set of observations. At station 6, 8, 10, and 11 corresponding to (30 km, 40 km, 50 km, and 55 km) respectively, the first round of observation deviates incrementally compared to the second and the third round of observations. At other stations the differences were very minimal but a bit more noticed in others. A glimpse of the linear graphical illustrations shows a continuous increase in the positioning accuracy from 5 km to 75 km with values ranging from 0.01 m to about 0.05 m.

Figure 6 shows the rms accuracies of the three observation sessions. At station 3 (15 km), little deviation exists among the three set of observations. At station 6, 8, 10, and 11 corresponding to (30 km, 40 km, 50 km, and 55 km) respectively, the first round of observation deviates incrementally compared to the second and the third round of observations. At some stations the difference is high but at other stations the differences were very minimal. A critical look at the linear graphical illustrations shows a continuous increase in the positioning accuracy from 5 km to 75 km, recorded values ranging from 0.01 m to 0.06 m.

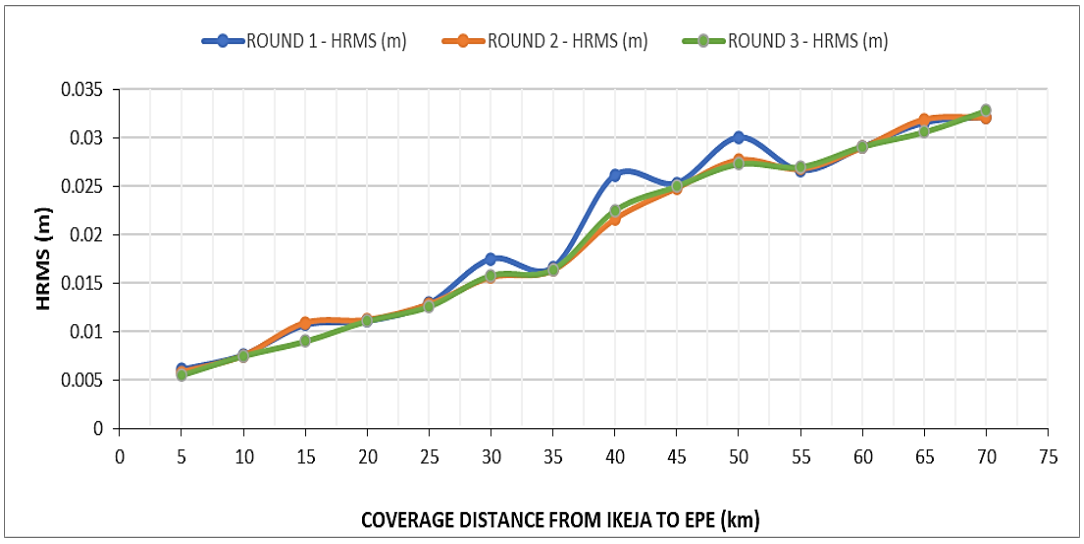

Figure 4: Horizontal accuracy for three rounds of observations

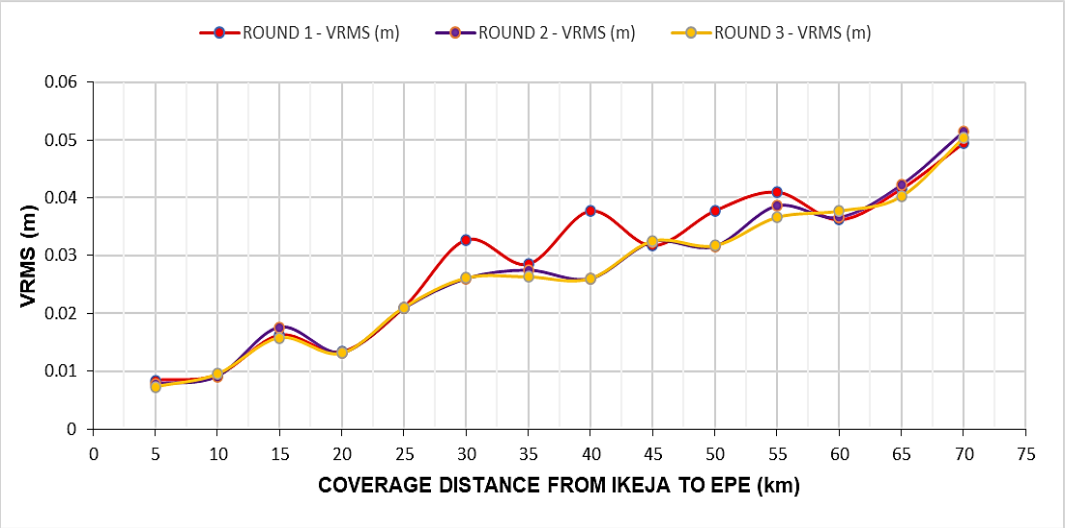

Figure 5: Vertical accuracy for three rounds of observations

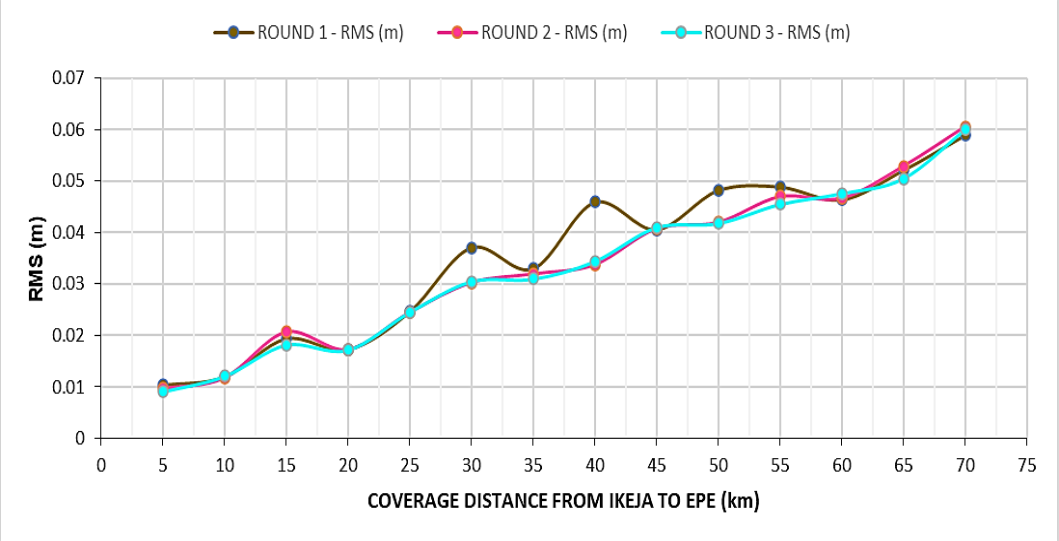

Figure 6: RMS accuracy for three rounds of observations

3.2 Linear Regression Modelling Results

The result presented in Table 5 contains the average RMS error attributed to the respective distances from the STGBC, while in Table 6, the summary of the regression analysis is presented. The multiple regression is the Pearson correlation coefficient between the distance coverage (independent variable) in kilometer and the RMS error (dependent variable) in positioning. There is a very strong positive relationship or correlation between the coverage distance and the RMS error in relative positioning to the STGBC. The R-square is the coefficient of determination which tells how much variation in the dependent variable is accounted for by the independent variables. In this case, the result shows that 97.79% of the RMS error in relative positioning is caused by the distance coverage of the GNSS rover away from the STGBC. The standard error is another important factor in the regression modelling. The standard error of the regression model is approximately 0.00241 m. This means the result obtained is very precise.

3.3 One-Way Analysis of Variance (ANOVA) Result

The analysis of variance (ANOVA) was carried out to determine if there are any significant differences between the means of three independent observations rms error. The result is presented in Table 7 and it is obvious that the P value is less than the significance value α, as such the null hypothesis is rejected and the alternative hypothesis is accepted. Therefore, there is a linear relationship between the distance coverage and the RMS error in relative positioning to the STGBC at 95% confidence interval (α = 0.05 significant value).

Table 5: Three Rounds Average Rms Error

Station	Coverage distance (Km)	Average rms (m)
1	5	0.00973
2	10	0.01196
3	15	0.01943
4	20	0.01726
5	25	0.02453
6	30	0.03263
7	35	0.03200
8	40	0.03803
9	45	0.04080
10	50	0.04400
11	55	0.04713
12	60	0.04690
13	65	0.05183
14	70	0.05983

Table 6: Linear Regression Statistics Summary		
S/No:	Parameters	Obtained value
1	Multiple R	0.98890
2	R-Square	0.97792
3	Adjusted R-Square	0.97608
4	Standard Error	0.00241
5	Observations	14

Table 7: Linear Regression ANOVA					
	df	SS	MS	F	Significance F (P Value)
Regression	1	0.003079302	0.003079302	531.6357	2.63452×10^{-11}
Residual	12	6.95055×10^{-5}	5.79213×10^{-6}		
Total	13	0.003148807			

3.4 Model Prediction

The regression model was used to predict the RMS error for distances up to 120 km away from the STGBC. The intercept and the coefficient of the regression model is shown in Table 8. The plot in Figure 7 will make it realistic to predict for any available value of the dependent variable (y) for the independent variable (x) with the constant term.

Figure 7 shows the regression plot and the equation of line of best fit for the linear relationship that could be used for the prediction of other distances above the 70 km radius from the STGBC. This equation is instrumental in the production of Table 9 consisting of the coverage distances, predicted average RMS, residual, and standard residual where available. The values highlighted in red colour (i.e. 75 km to 120 km) signify the consistency of the analysis as the RMS error steadily increases as distances increases away from the STGBC.

The precision of the model is ascertained with the display of the scattered plot of the residuals Figure 8. The standard residual values computed in Table 9 are used to determine if there are any potential outliers in the observed dataset. The standard residual value should be between -3 and +3. Any value that goes beyond the range is counted as outlier. The review of the results indicates there are no outliers.

Table 8: Linear Regression Model Intercept and Coefficient								
	Coefficients	Standard error	t-Stat	P-value	Lower 95%	Upper 95%	Lower 95.0%	Upper 95.0%
Intercept	0.00641	0.001358	4.72118	0.000496	0.00345	0.00937	0.003454	0.009374
Coverage (Km)	0.00073	3.19123×10^{-5}	23.05722	2.63×10^{-11}	0.000666	0.00080	0.00066	0.000805

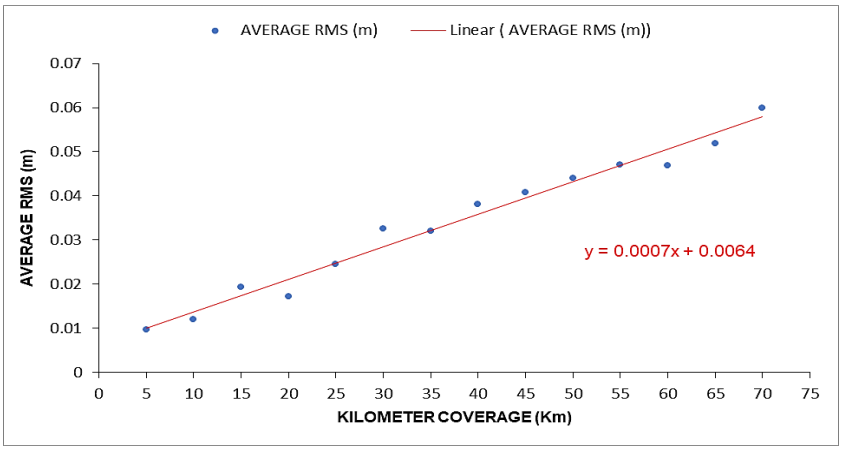

Figure 7: The regression model line of best fit for the prediction

Table 9: Linear Regression Model Residual			
Coverage distance (Km)	Predicted average rms (m)	Residuals	Standard Residuals
5	0.010093333	-0.00036	-0.155691362
10	0.013772381	-0.001805714	-0.780928099
15	0.017451429	0.001981905	0.857126252
20	0.021130476	-0.00386381	-1.671004904
25	0.024809524	-0.00027619	-0.119445754
30	0.028488571	0.004144762	1.792510067
35	0.032167619	-0.000167619	-0.072491216
40	0.035846667	0.002186667	0.945680863
45	0.039525714	0.001274286	0.551097994
50	0.043204762	0.000795238	0.343921394
55	0.04688381	0.000249524	0.10791306
60	0.050562857	-0.003662857	-1.584097821
65	0.054241905	-0.002408571	-1.041649347
70	0.057920952	0.001912381	0.827058873
75	0.061600036		
80	0.065279086		
85	0.068958136		
90	0.072637186		
95	0.076316236		
100	0.079995286		
105	0.083674336		
110	0.087353386		
115	0.091032436		
120	0.094711486		

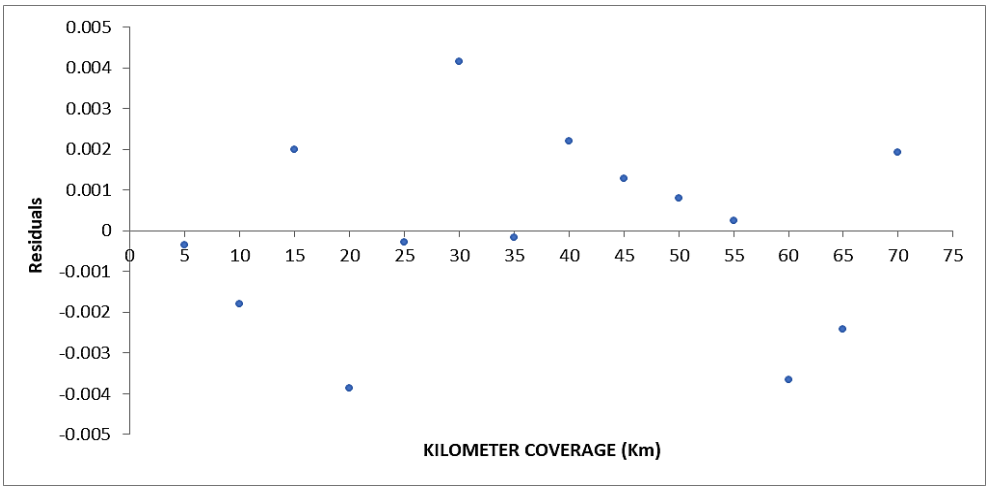

Figure 8: Scattered Plot of residuals from the linear regression model.

Table 10: The Probability Output of The Linear Regression

Percentile	Average rms (m)
3.571428571	0.009733333
10.71428571	0.011966667
17.85714286	0.017266667
25.00000000	0.019433333
32.14285714	0.024533333
39.28571429	0.032000000
46.42857143	0.032633333
53.57142857	0.038033333
60.71428571	0.040800000
67.85714286	0.044000000
75.00000000	0.046900000
82.14285714	0.047133333
89.28571429	0.051833333
96.42857143	0.059833333

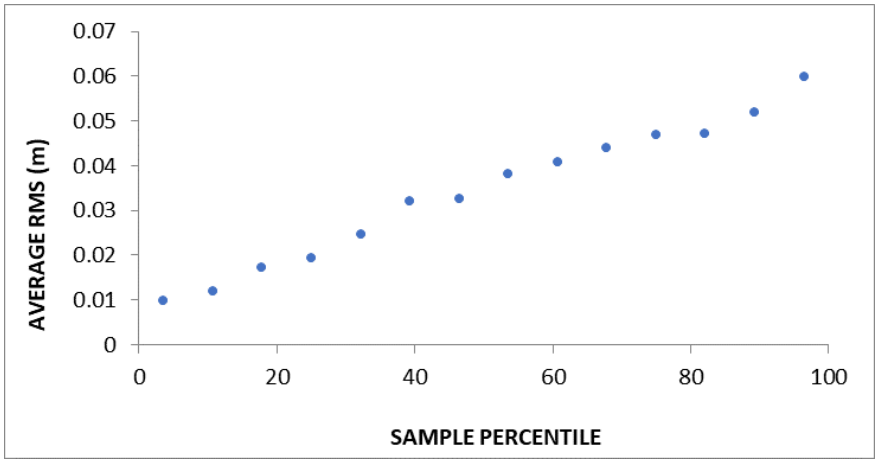

Figure 9: Normal probability distribution plot

To determine if our observation dataset (the average RMS error of positioning) is normally distributed, the probability plot shown in Figure 9 was plotted.

The spread of the average RMS error in positioning with respect to the percentile plot indicates that the data collected from the field observations are normally distributed.

3.5 Model Performance Testing Using Known Controls

Haven formulated the regression model for predicted RMS positioning error when carrying our RTK observations with reference to STGBC, we decided to test the model performance on existing known control points in Lagos State. Table 11 contains the control points identification number, the 3D coordinates, and the errors components.

Table 11: RTK Positioning Referenced to STGBC

Control_ID	Observed Northings (m)	Observed Eastings (m)	Observed Orthometric Height (m)	hrms	vrms	rms	Location
XST117	725348.0213	540603.7682	29.1091	0.0057	0.0073	0.0093	Idiroko, Lagos
XST118	729878.4443	538335.1327	35.5037	0.0053	0.0077	0.0093	Balogun Street, Ikeja Lagos

Table 12: Test Results from The Regression Model on Known Controls

Control_ID	Distance to CORS (Km)	Predicted rms (m)	Observed rms (m)	Residual
XST117	3.873	0.009264078	0.0093	-3.59219×10^{-5}
XST118	1.219	0.007311238	0.0093	-0.001988762

The results in Table 12 show the applicability of the model in predicting and estimating positioning error. The rms predicted from the linear regression model reveals close values with the values of rms observed on the field, the residual in turn is very negligible.

4. Conclusions

This research work has justified that surveying activities referenced to the STGBC are reliable in terms of both accuracy and precision. The One-Way ANOVA analysis confirmed the consistency in the repeated observations using the STGBC as reference. This implies that surveying activities such as staking out operation, electricity tower spotting ranging, and pipeline ranging operations etc. can be carried out effectively using the STGBC around Lagos State and beyond. Through the linear regression analysis, it is easy to justify statistically the relationship between RMS error in positioning and the distance coverage with the use of the GNSS rover. This regression model can provide room for reconnaissance surveys information whenever surveying activities are required with respect to the CORS station. The predicted result using the model could serve as guide geospatial professionals to have clear understanding of the expected positioning accuracy even before going to the site. We would therefore recommend that geospatial expert should take advantage of the existing STGBC in Nigeria for their surveying and mapping activities.

Declaration of Competing Interest

The authors declare no completing interest as regards every aspect of this research.

References

Agca, M., Daloglu, A.I., 2023. Local Geoid height calculations with GNSS, airborne, and spaceborne Lidar data. Egypt. J. Rem. Sens. Spa. Sci. 26, Pp. 85–93. https://doi.org/10.1016/j.ejrs.2022.12.009

Botsyo, S., Bortei, B.B., Ayer, J., 2020. CORS usage for GPS survey in the greater Accra region: Advantages, Limitation, and Suggested Remedies. J. geovis. spat. anal., 4, Pp. 20. https://doi.org/10.1007/s41651-020-00061-8

Dai, W., Liu, B., Meng, X., Huang, D., 2014. Spatio-temporal modelling of dam deformation using independent component analysis. Surv Rev., 46 (339), Pp. 437–443.

Erekosima, M., Onoriode, B., 2018. GPS CORS Technology Implementation in the Oil Industry- Benefits and Challenges. Embracing our smart world where the continents connect: enhancing the geospatial maturity of societies (9459) FIG Congress. Istanbul, Turkey, Pp. 6–11.

European Space Agency, 2018. RTK Fundamentals, navipedia. Retrieved May 31, 2023 from http://www.navipedia.net/index.php/RTK_Fundamentals.

Ferreira, L.B, da Cunha, F.F., Zanetti, S.S., 2021. Selecting models for the estimation of reference evapotranspiration for irrigation scheduling purposes. PLoS ONE, 16 (1), Pp. e0245270. https://doi.org/10.1371/journal.pone.0245270

Fortia, V.V., Marcelo, D.F., 2019. Optimal linear mean square filter for the operation mode of continuous-time Markovian jump linear systems. IET Control Theory and Applications, doi: 10.1049/IET-CTA.2018.5659

Fotiou, A., Pikridas, C., Chatzinikos, M., 2006. Long distance GPS baseline solutions using various software and EPN data. Munich, Germany: XXIII FIG congress-shaping the change.

Hamish, R., 2004. The repeatability of the height component of short GPS baselines as a function of distance. New Zealand: University of Otago, Dunedin.

Hernández-Andrade, D., Romero-Andrade, R., Sharma, G., Trejo-Soto, M.E., Cabanillas-Zavala, J.L., 2022. Quality assessment of continuous operating reference stations (CORS) - GPS stations in Mexico. Geod. and Geodyn., 13 (3), Pp. 275-287. https://doi.org/10.1016/j.geog.2021.12.003.

Homayoon, G., Takamitsu, K., 2019. Error propagation approach for estimating root mean square error of the reference evapotranspiration when estimated with alternative data.. Journal of Agricultural Engineering, doi: 10.4081/JAE.2019.909

Hu, Q., Linlin, X., Xinyu, C., 2018. A CORS-Based Differential Correction Approach for AIS Mobile Stations" Sensors 18 (11), Pp. 3626. https://doi.org/10.3390/s18113626

Jaskowski, P., Tomczuk, P., Chrzanowicz, M., 2022. Construction of a measurement system with GPS RTK for operational control of street lighting. Energies, 15, Pp. 9106. https://doi.org/10.3390/en15239106.

Jing-xiang, G., Hong, H., 2009. Advanced GNSS technology of mining deformation monitoring. The 6th International Conference on Mining Science & Technology. Procedia Earth and Planetary Science 1-2009, Pp. 1081–1088.

Khai, P.C., Long N.Q., 2019. Accuracy assessment of the single CORS technology for establishing the largescale cadastral map. International Journal of Scientific & Engineering Research 10 (5), 1 ISSN 2229-5518 IJSER. http://www.ijser.org

Kolopaking, S.A., 2018. Threat Modeling and Countermeasures of Continuously Operating Reference Stations Network Backbone to Improve Precise Positioning Service Security. Master Dissertation. Graduate School of System Design and Management, Keio University Major in System Engineering.https://koara.lib.keio.ac.jp/xoonips/modules/xoonips/detail.php?koara_id=K040002001-00002017-0026

Lau, L., Kai-Wing T., 2023. A Data Quality Assessment Approach for High-Precision GNSS Continuously Operating Reference Stations (CORS) with Case Studies in Hong Kong and Canada/USA" Remote Sensing 15 (70), Pp. 1925. https://doi.org/10.3390/rs15071925

Li, Z., Zhang, T., Qi, F., Tang, H., Niu, X., 2019. Carrier phase prediction method for GNSS precise positioning in challenging environment, Adv. in Spa. Res., 63 (7), Pp. 2164-2174. https://doi.org/10.1016/j.asr.2018.12.015.

Liu, B., Dai, W., Peng, W., 2015. Spatiotemporal analysis of GPS time series in vertical direction using independent component analysis. Earth Planet Sp., 67, Pp. 189. https://doi.org/10.1186/s40623-015-0357-1

Long, S.A.T., 1974. Derivation of formulas for root-mean-square errors in location, orientation, and shape in triangulation solution of an elongated object in space. Report number: NASA TN D-7477. https://ntrs.nasa.gov/api/citations/19740018170/downloads/19740018170.pdf

Mendez-Astudillo, J., Lau, L., Tang, Y.T., Moore, T., 2021. A new global navigation satellite system (GNSS) based method for urban heat island intensity monitoring. Int'l J. of Appl. Earth Observ. and Geoinf., 94, Pp. 102222. https://doi.org/10.1016/j.jag.2020.102222

National Geodetic Survey NGS, 2021. NOAA CORS Network (NCN) CORS FAQs. Retrieved January 8, 2023 from https://geodesy.noaa.gov/CORS/cors_faqs.shtml

Nordin, N.Ab.N., Mustapa, N.B., Satar, A.B.A., 2021. Ability of RTK-based GPS measurement method in high accuracy work in geomatics study. Asian J. of Uni. Edu. (AJUE) 17 (4). https://doi.org/10.24191/ajue.v17i4.16212.

Oladosu, S.O., Ehigiator-Irughe, R., Muhammad, M.B.M.E., 2022. Establishment and Validation of Continuously Operating Reference Stations Geosystems Network on Static and Real-Time Kinematic in Benin City, Nigeria J. Appl. Sci. Environ. Manage., 26 (5), Pp. 801-808. DOI: https://dx.doi.org/10.4314/jasem.v26i5.4

Omogunloye, O.G., Okorocha, C.V., Ojegbile, B.M., Odumosu, J.O., Ajayi, O.G., 2017. Comparative analysis of the standard error in relative GNSS positioning for short, medium and long baselines. J. of Geomat., 11

(2), Pp. 207-217. https://isgindia.org/wp-content/uploads/2017/10/JoG_1102_08.pdf

Paquet P., 1980. Variations of Doppler results with software and time. Philosophical transactions - Royal Society. Mathematical, physical and engineering sciences, doi: 10.1098/RSTA.1980.0029

Pirti, A., Hosbas, R.G., 2019. Role of CORS RTK (Network RTK) mode measurements: In determination of the forest boundary: A Case Study of ISKI-CORS. forestry ideas, 25 (2), (58), Pp. 394–403.

Shuguang, W., Guigen, N., Haiyang, L., 2017. Characteristics of Coordinate Time Series of Shenzhen Continuously Operating Reference Stations. doi: 10.1007/978-981-10-4588-2_19

Wu, S., Nie, G., Li, H., 2017. Characteristics of Coordinate Time Series of Shenzhen Continuously Operating Reference Stations. In: Sun, J., Liu, J., Yang, Y., Fan, S., Yu, W. (eds) China Satellite Navigation Conference (CSNC) 2017 Proceedings: Volume I. CSNC 2017. Lecture Notes in Electrical Engineering, vol 437. Springer, Singapore. https://doi.org/10.1007/978-981-10-4588-2_19